PCCP

PAPER

Cite this: *Phys. Chem. Chem. Phys.*, 2020, **22**, 10027

Reaction mechanism, energetics, and kinetics of the water-assisted thioformaldehyde + •OH reaction and the fate of its product radical under tropospheric conditions†

Parandaman Arathala, Mark Katz and Rabi A. Musah *

The reactions of thioformaldehyde (H_2CS) with OH radicals and assisted by a single water molecule have been investigated using high level *ab initio* quantum chemistry calculations. The H_2CS + •OH reaction can in principle proceed through: (1) abstraction, and (2) addition pathways. The barrier height for the addition reaction in the absence of a catalyst was found to be −0.8 kcal mol^{-1}, relative to the separated reactants, which has a ∼1.0 kcal mol^{-1} lower barrier than the abstraction channel. The H_2CS + •OH reaction assisted by a single water molecule reduces the barrier heights significantly for both the addition and abstraction channels, to −5.5 and −6.7 kcal mol^{-1} respectively, compared to the un-catalyzed H_2CS + •OH reaction. These values suggest that water lowers the barriers by ∼6.0 kcal mol^{-1} for both reaction paths. The rate constants for the $H_2CS\cdots H_2O$ + •OH and $OH\cdots H_2O$ + H_2CS bimolecular reaction channels were calculated using Canonical Variational Transition state theory (CVT) in conjunction with the Small Curvature Tunneling (SCT) method over the atmospherically relevant temperatures between 200 and 400 K. Rate constants for the H_2CS + •OH reaction paths for comparison with the H_2CS + •OH + H_2O reaction in the same temperature range were also computed. The results suggest that the rate of the H_2CS + •OH + H_2O reaction is slower than that of the H_2CS + •OH reaction by ∼1–4 orders of magnitude in the temperatures between 200 and 400 K. For example, at 300 K, the rates of the H_2CS + •OH + H_2O and H_2CS + •OH reactions were found to be 2.2 × 10^{-8} s^{-1} and 6.4 × 10^{-6} s^{-1}, respectively, calculated using [OH] = 1.0 × 10^6 molecules cm^{-3}, and [H_2O] = 8.2 × 10^{17} molecules cm^{-3} (300 K, RH 100%) atmospheric conditions. Electronic structure calculations on the $H_2C(OH)S$• product in the presence of $^3O_2$ were also performed. The results show that H_2CS is removed from the atmosphere primarily by reacting with •OH and O_2 to form thioformic acid, HO_2, formaldehyde, and SO_2 as the main end products.

Received 1st February 2020,
Accepted 7th April 2020

DOI: 10.1039/d0cp00570c

rsc.li/pccp

1. Introduction

Compounds that contain carbon–sulfur bonds are commonly observed in atmospheric, combustion, and biological chemistry. Thioformaldehyde (H_2CS) is the simplest thiocarbonyl-containing volatile organosulfur compound (VOSC). While it is highly unstable with a short lifetime of only few minutes at low pressures,[1] and readily polymerizes into a cyclic trimer, it is of significant importance.[2–5] Several astrochemistry research groups have reported the detection of monomeric thioformaldehyde in dark and interstellar clouds.[6–8] For example, it was detected for the first time in the circumstellar envelope around an asymptotic giant branch (AGB) star.[9] Spectral bands representative of H_2CS were detected in the Orion KL nebula[10] and in the atmosphere of the comet Hale–Bopp.[11] It is also believed that H_2CS can play a significant role in the photochemical evolution growth of sulfur containing molecules in the Earth's atmosphere and other astronomical systems.[6–12] Several experimental studies[13,14] have been performed on monomeric H_2CS to investigate the vibrational[15–24] and rotational spectra[1,19–21,23] of its ground and excited electronic states.[24,25] The observations of these studies have been complemented with the results

University at Albany—State University of New York, Department of Chemistry, 1400 Washington Avenue, Albany, NY 12222, USA. E-mail: rmusah@albany.edu

† Electronic supplementary information (ESI) available: Tables S1–S19, which present the optimized geometries of all the stationary points, their vibrational frequencies and rotational constants, relative energies with respect to starting reactants, calculated total electronic energies including zero-point energy corrections, and imaginary frequencies of various TSs as discussed in the text at different levels of theory, temperature dependent unimolecular and bimolecular rate constants using CVT/SCT method, equilibrium constants, tunneling contributions for each reaction paths, *T*1 diagnostic values for all the stationary points in the $H_2C(OH)S$• + $^3O_2$ reaction, and the optimized geometries of the thioformaldehyde + •OH reaction catalyzed by the water dimer molecule. See DOI: 10.1039/d0cp00570c

of quantum chemistry investigations of H_2CS.[26–29] The data obtained have provided fundamental insights into the physical chemistry of thioformyl and similar sulfur-containing molecules. The high polarizability and reactivity of the thioformyl functional group in H_2CS facilitates the formation of new C–C bonds.[30] Various experimental and theoretical studies of the $CH_3S^\bullet$ + O_2 reaction suggest that H_2CS is formed as a final byproduct,[31–33] and it is currently believed that formation of thiocarbonyl compounds in the atmosphere occurs *via* nucleophilic addition of HS^- to the carbonyl group.[34] However, the results of recent theoretical calculations indicate that the gas phase reaction of the simplest Criegee intermediate (CH_2OO) or formaldehyde (CH_2O), with hydrogen sulfide (H_2S) catalyzed by water or organic acids, also can lead to the formation of H_2CS in the atmosphere.[34,35] These studies suggest that the formation of H_2CS under acidic conditions is more energetically favorable.[34] They also support the gas phase existence of H_2CS in the atmosphere *via* release from various sources. Therefore, it is important to study the reactivity of H_2CS towards environmentally relevant free radicals such as $^\bullet$OH, in order to reveal information about its fate in the atmosphere.

To date, there are no reports on the atmospheric oxidation of H_2CS, even though it can react rapidly with major atmospheric oxidants such as OH radical. The H_2CS + $^\bullet$OH reaction can proceed *via* two reaction pathways: (1) direct hydrogen abstraction from H_2CS by the OH radical to form $H^\bullet CS$ + H_2O; and (2) OH radical attack on the sp^2-hybridized C atom to form the $H_2C(OH)S^\bullet$ radical (eqn (1) and (2))

$$H_2CS + {}^\bullet OH \rightarrow H^\bullet CS + H_2O \quad (1)$$

$$H_2CS + {}^\bullet OH \rightarrow H_2C(OH)S^\bullet \quad (2)$$

However, it has recently been suggested that water, being the third most abundant species present in the atmosphere, is capable of catalyzing various atmospheric reactions.[34] Over the last few years, several research groups have been studying the catalytic effect of a single water molecule on various atmospheric reactions.[36–40] For example, it has been reported that a single water molecule acts as a catalyst in $^\bullet$OH + H_2CO, $^\bullet$OH + CH_2CH_2, $^\bullet$OH + CH_2NH, and HNCO + $(CH_3)_2NH$ reactions.[36,38,40] The data from these studies suggest that a single water molecule significantly reduces the reaction barrier, and does not increase the rate of reaction at atmospherically relevant temperatures.[37,38,40] There are no previous reports of investigations of the reaction mechanism, energetics and kinetics of the H_2CS + $^\bullet$OH reaction assisted by single water molecule. In this work, we have studied this reaction to reveal these details using high level computational methods. The possible abstraction and addition channels for the H_2CS + $^\bullet$OH reaction assisted by a single water molecule are presented below as eqn (3) and (4) respectively.

$$H_2CS + {}^\bullet OH + H_2O \rightarrow H^\bullet CS + 2H_2O \quad (3)$$

$$H_2CS + {}^\bullet OH + H_2O \rightarrow H_2C(OH)S^\bullet + H_2O \quad (4)$$

We investigated the H_2CS + $^\bullet$OH reaction in the presence of a single water molecule by calculating the energies with high level computational methods. We also explored, by the small curvature tunneling (SCT) method,[41] the reaction kinetics using canonical variational transition state theory (CVT).[42,43] The observed results were then compared to the energetics and kinetic results obtained from analysis of the H_2CS + $^\bullet$OH reaction in the absence of the water catalyst (*i.e.* eqn (1) and (2)). It was found that the addition reaction to form the $H_2C(OH)S$ radical is more dominant than abstraction. We then determined the atmospheric fate of the $H_2C(OH)S$ radical in the presence of molecular oxygen ($^3O_2$). This reaction leads to the formation of thioformic acid, HO_2, SO_2, and formaldehyde as final products in the atmosphere.

2. Computational methods

Quantum chemistry calculations on the gas phase reactions of H_2CS with $^\bullet$OH alone and with H_2O as a catalyst were carried out using the Gaussian-16 program suite.[44] All of the stationary points on the potential energy surface (PES) were optimized using both density functional theory (DFT) and second order Møller–Plesset perturbation theory (MP2).[45] The DFT method calculations were performed using the M06-2X hybrid meta density functional,[46] which has been shown to produce good results for developing reaction mechanisms and for conducting rate constant calculations.[33,47,48] A large Pople type basis set 6-311++G(3df,3pd) was used at the M06-2X theory level, and the cc-pVTZ basis set was used at the MP2 level of theory. No basis set superposition error (BSSE) corrections were done in this work by the counterpoise (CP) correction method. This is because of the difficulty of applying BSSE corrections in a uniform manner to all the molecules involved throughout the reaction mechanism. The keyword OPT = TS, CALCFC commands developed in Gaussian-16 was used to optimize all of the transition states (TSs) observed in this work. The existence of TSs, reactant complexes (RCs) and product complexes (PCs) on the PESs was further validated by intrinsic reaction coordinate (IRC) calculations[49,50] carried out at the M06-2X/6-311++G(3df,3pd) level for the TSs optimized at the same theory level. The reactants, RCs, PCs, dimers, and trimers labelled as pre-reactive complexes (PRCs), and products were identified with no imaginary frequencies and all the TSs were identified with one imaginary vibrational frequency. The energies of all the calculated stationary points were further developed by calculating the single point energies using the coupled cluster single and double substitution method with a perturbative treatment of triple excitation (CCSD(T))[51] coupled with the aug-cc-pVTZ basis set on the optimized geometries at both the M06-2X/6-311++G(3df,3pd), and MP2/cc-pVTZ levels. This combination was used because these methods have been previously employed in a number of studies involving reactions of sulfur compounds with OH radicals.[52–56]

The CCSD(T)/aug-cc-pVTZ//M06-2X/6-311++G(3df,3pd) (designated as CCSD(T)//M06-2X) and CCSD(T)/aug-cc-pVTZ//MP2/cc-pVTZ (designated as CCSD(T)//MP2)) levels of theory typically give energy values accurate to $\sim$1.6 kcal mol^{-1} and $\sim$1.4 kcal mol^{-1}, respectively. This was predicted by calculating the enthalpy of the

reaction $H_2CS + {}^{\bullet}OH \rightarrow H{}^{\bullet}CS + H_2O$, which was found to be -24.6 kcal mol^{-1} and -21.6 kcal mol^{-1} computed at the CCSD(T)//M062X and CCSD(T)//MP2 levels respectively. These two values agree with the experimentally measured[57,58] enthalpy of reaction, which was calculated to be $\sim -23 \pm 0.5$ kcal mol^{-1}. Therefore, the computed and experimentally measured values are within $\sim$1.6 and $\sim$1.4 kcal mol^{-1}, respectively at both levels. This gives greater confidence in the energy calculations for all the reaction paths involving $H_2CS + {}^{\bullet}OH$ in the presence and absence of the water catalyst. The spin expectation value $\langle S^2 \rangle$ for each species at the M06-2X and MP2 levels were found to be $\sim$0.75–0.79 and $\sim$0.75–0.95, respectively. These values indicate that the spin contamination predicted at the MP2 level is higher than that obtained by M06-2X calculations, which leads to the zero-point energy calculated at the MP2 level having more uncertainty.[59] Therefore, we used energies computed at the CCSD(T)//M06-2X level in all the PESs and rate constant calculations, unless otherwise stated. The calculated total electronic energies (E_{total}) together with the zero-point energies (ZPE) and the corrected electronic energies [E_{total}(ZPE)] for all the reactants, intermediates, TSs, and products obtained at the various levels (M06-2X, MP2, and CCSD(T)) are presented in Tables S1–S3 (ESI†). The optimized geometries, relative energies of the stationary points obtained at the various levels of theory, vibrational frequencies, rotational constants, and imaginary frequencies of all the transition states are also provided in the ESI† (Tables S4–S11).

3. Results and discussion

3.1. Energies and stationary points on the potential energy surface

Electronic structure calculations of all the stationary points on the potential energy surfaces (PESs) involved in the water-free and water-assisted $H_2CS + {}^{\bullet}OH$ reactions through abstraction and addition channels were performed with high level CCSD(T)//M06-2X and CCSD(T)//MP2 computational methods. The relative energies of all the stationary points present on the PESs at both levels are given in Table S4 of the (ESI†). The relative energy data in Table S4 (ESI†) for the $H_2CS + {}^{\bullet}OH$ reaction alone and in the presence of water clearly show that the range of the deviation from one another of the energies between the M06-2X and MP2 levels is $\sim$1 to 5.0 kcal mol^{-1}. However, the energies obtained by the CCSD(T)//M06-2X and CCSD(T)//MP2 methods were in good agreement with one another, with a maximum deviation $\sim$3 kcal mol^{-1} for the HCS radical and up to 5 kcal mol^{-1} for some complexes for the two reaction systems (see Table S4, ESI†). Therefore, we used the energies computed at the CCSD(T)//M06-2X level throughout this work. First, we investigated the water-free $H_2CS + {}^{\bullet}OH$ reaction pathways computed at the CCSD(T)//M06-2X level, as shown in Fig. 1. The zero-point corrected energies of all the stationary points are given with respect to the starting reactants in Fig. 1. The optimized reactants, reactant complexes (RCs), transition states (TSs), product complexes (PCs) and products involved in the $H_2CS + {}^{\bullet}OH$ reaction are given in Fig. 2.

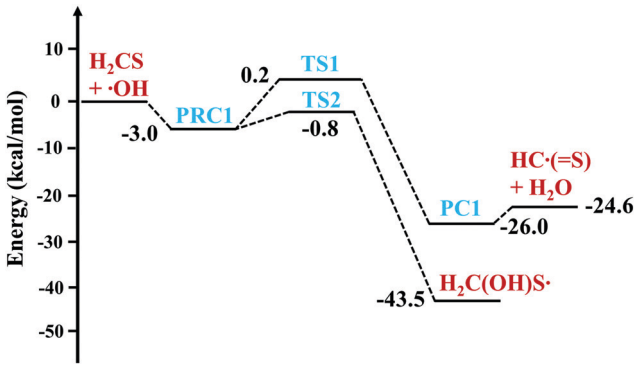

Fig. 1 Potential energy surface diagram for the $H_2CS + {}^{\bullet}OH$ reaction without the water catalyst at the CCSD(T)/aug-cc-pVTZ//M06-2X/6-311++G(3df,3pd) level. The symbols are defined as follows: PRC1 ($H_2CS\cdots OH$ dimer), TS1, TS2 (transition states), and PC1 (product complex).

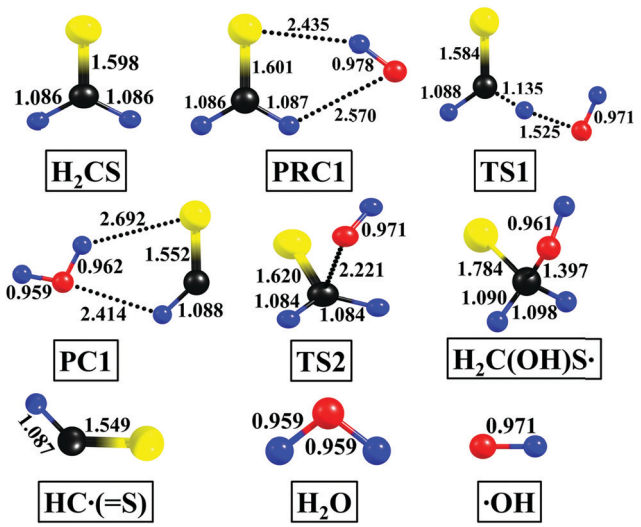

Fig. 2 Optimized geometries of the reactants, reactant complex (PRC1), transition states (TSs), product complex (PC), and products for the $H_2CS + {}^{\bullet}OH$ reaction obtained at the M06-2X/6-311++G(3df,3pd) level of theory. The yellow, black, and blue colors denote sulfur, carbon, and hydrogen atoms, respectively.

In Fig. 1, the reaction starts by forming a barrierless dimer complex (PRC1) with a binding energy of 3.0 kcal mol^{-1} relative to the separated reactants, and in which the O and H atoms of OH are involved in hydrogen bonding interactions with the H and S atoms of H_2CS (see Fig. 2), respectively. The O atom of OH in PRC1 approaches an H atom of H_2CS for abstraction to form TS1. The calculated barrier height for the hydrogen abstraction transition state (TS1) was computed to be 0.2 kcal mol^{-1} above the separated reactants at the CCSD(T)//M06-2X level. The formed TS1 passes through the product complex (PC1), which then leads to the formation of $H{}^{\bullet}CS + H_2O$ as products. The addition channel also proceeds through PRC1 to form a new C–O bond between the O atom of ${}^{\bullet}OH$ and the C atom of H_2CS, passing through TS2 as shown in Fig. 1 and 2. The computed barrier height for TS2 was found to be -0.8 kcal mol^{-1} below the starting

reactants (H_2CS + $^{\bullet}OH$). Therefore, the addition reaction barrier height is ~1.0 kcal mol^{-1} lower compared to that of the abstraction pathway. This reaction then proceeds to form $H_2C(OH)S^{\bullet}$ as the final product. From the barrier height data, we concluded that the addition pathway is more dominant when compared to the abstraction path. The barrier height for the addition path was computed to be −0.8 kcal mol^{-1} at the CCSD(T)//M06-2X level. This barrier height is ~5.4 kcal mol^{-1} and ~1.6 kcal mol^{-1} lower than the values for the H_2CO + $^{\bullet}OH$ and H_2CNH + $^{\bullet}OH$ addition reaction barrier heights respectively, and it has a comparable barrier height to the CH_2CH_2 + $^{\bullet}OH$ addition reaction computed at the CCSD(T)/aug-cc-pVTZ//BH&HLYP/aug-cc-pVTZ level.[60] Similarly, the H atom abstraction barrier height for the H_2CS + $^{\bullet}OH$ reaction is ~2.3 kcal mol^{-1}, and ~2.5 kcal mol^{-1} above, and ~4.5 kcal mol^{-1} below the values for the H_2CO + $^{\bullet}OH$, H_2CNH + $^{\bullet}OH$, and CH_2CH_2 + $^{\bullet}OH$ reactions respectively.[60]

We then investigated the effect of a single water molecule on the H_2CS + $^{\bullet}OH$ reaction. The simultaneous collision of isolated $^{\bullet}OH$, H_2CS and H_2O molecules is unlikely in the atmosphere. Instead, the reaction occurs first through the formation of dimer complexes, which then collide with a third isolated reactant species, leading to the following three possible bimolecular water assisted H-abstraction reaction pathways (5a)–(5c):

$$H_2CS\cdots H_2O + {}^{\bullet}OH \rightarrow H{}^{\bullet}CS + 2H_2O \quad (5a)$$

$$H_2CS + OH\cdots H_2O \rightarrow H{}^{\bullet}CS + 2H_2O \quad (5b)$$

$$H_2CS\cdots OH + H_2O \rightarrow H{}^{\bullet}CS + 2H_2O \quad (5c)$$

The PESs involving all the stationary points for the abstraction and addition paths of H_2CS + $^{\bullet}OH$ assisted by a single water molecule are shown in Fig. 3, and all the optimized structures are presented in Fig. 4. The energies of all the stationary points on the PESs were calculated at the CCSD(T)//M06-2X level. We found three possible dimer complexes with H_2CS, $^{\bullet}OH$, and H_2O as reactants, all of which are stabilized by hydrogen bonding interactions. The optimized most stable structures and the relative stabilities of the dimer complexes such as $H_2CS\cdots OH$ (PRC1), $H_2CS\cdots H_2O$ (PRC2), and $HO\cdots H_2O$ (PRC3) are shown in Fig. 2, 4, and Table S4 of the ESI.† The binding energies of PRC1, PRC2 and PRC3 were calculated to be 3.0, 3.1 and 3.9 kcal mol^{-1} at the CCSD(T)//M06-2X level, which agrees well with previously reported values.[34,37] The formed dimer complexes can react by colliding with the other isolated reactant molecule as shown in eqn (5a)–(5c), and these are presented as entrance channels in Fig. 3. The reactions, starting from H_2CS + $^{\bullet}OH$ + H_2O separated reagents, and the bimolecular collisions such as $H_2CS\cdots OH$ + H_2O, $H_2CS\cdots H_2O$ + $^{\bullet}OH$ and H_2CS + $OH\cdots H_2O$, lead to the formation of a three-body reactant complex (RC1) which is −9.5 kcal mol^{-1} below the energy of the starting reactants as shown in Fig. 3. The impact of each elementary reaction given in eqn (5a)–(5c) depends on the atmospheric concentration of the respective dimer complex. Based on the binding energies of the $H_2CS\cdots OH$, $H_2CS\cdots H_2O$, and $OH\cdots H_2O$ dimers and the average atmospheric concentrations of each reactant species involved in their formation, RC1 *via* the $H_2CS\cdots OH$ + H_2O reaction pathway may be negligible. This is because $^{\bullet}OH$ and H_2CS are present in lower amounts in the atmosphere when compared to water, and hence formation of the $H_2CS\cdots OH$ dimer may not occur to a significant degree when compared to other possible dimers in the atmosphere. Therefore, we considered the $H_2CS\cdots H_2O$ + $^{\bullet}OH$ and H_2CS + $OH\cdots H_2O$ pathways only. The reaction then proceeds from RC1 through a seven membered ring transition state (TS3) to product complex (PC2) formation, which undergoes unimolecular decomposition to form $H{}^{\bullet}CS$ + $2H_2O$ as separated products. Interestingly, the barrier height for this reaction was found to be −5.5 kcal mol^{-1} below the H_2CS + $^{\bullet}OH$ + H_2O separated reactants. This value suggests that H atom abstraction from H_2CS by $^{\bullet}OH$ in the presence of a single water molecule reduces the barrier height by ~5.7 kcal mol^{-1} compared to the H_2CS + $^{\bullet}OH$ reaction in the absence of water. We also found another transition state (TS3a) for the H abstraction reaction corresponding to an alternative arrangement in which the water and OH radical positions are interchanged compared to that in TS3, as shown in Fig. 4. The alternative arrangement TS3a barrier height was found to be 0.8 kcal mol^{-1} above the starting reagents. The structure of TS3a is shown in Fig. 4. This alternative configuration has a 6.3 kcal mol^{-1} higher barrier compared to that of TS3. Therefore, it was not considered in the rate constant calculations.

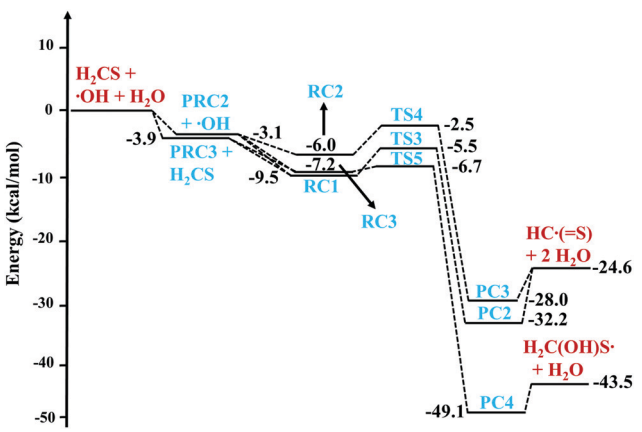

Fig. 3 Potential energy surface diagram for the H_2CS + $^{\bullet}OH$ reaction assisted by a single water molecule assisted by a single water molecule obtained at the CCSD(T)/aug-cc-pVTZ//M06-2X/6-311++G(3df,3pd) level. The symbols are defined as follows: PRC2 ($H_2CS\cdots H_2O$ dimer), PRC3 ($HO\cdots H_2O$ dimer), RC1, RC2, RC3 (reactant complexes), TS3, TS4, TS5 (transition states), and PC2, PC3, PC4 (product complexes).

As shown in Fig. 3, the aforementioned abstraction channel is also possible by collision of the $H_2CS\cdots H_2O$ dimer with OH radical to form a barrierless reactant complex (RC2). The OH and H_2O moieties are separated from each other in RC2, while in RC1, the OH and H_2O moieties are held together by hydrogen bonds in a ring-like formation (see Fig. 4). The present CCSD(T)//M06-2X calculations indicate that the binding energy of RC2 is 6.0 kcal mol^{-1} below that of the separated reagents. This value suggests that RC2 is higher in energy than RC1 by 3.5 kcal mol^{-1}. RC2 passes through TS4 with a barrier height of −2.5 kcal mol^{-1}

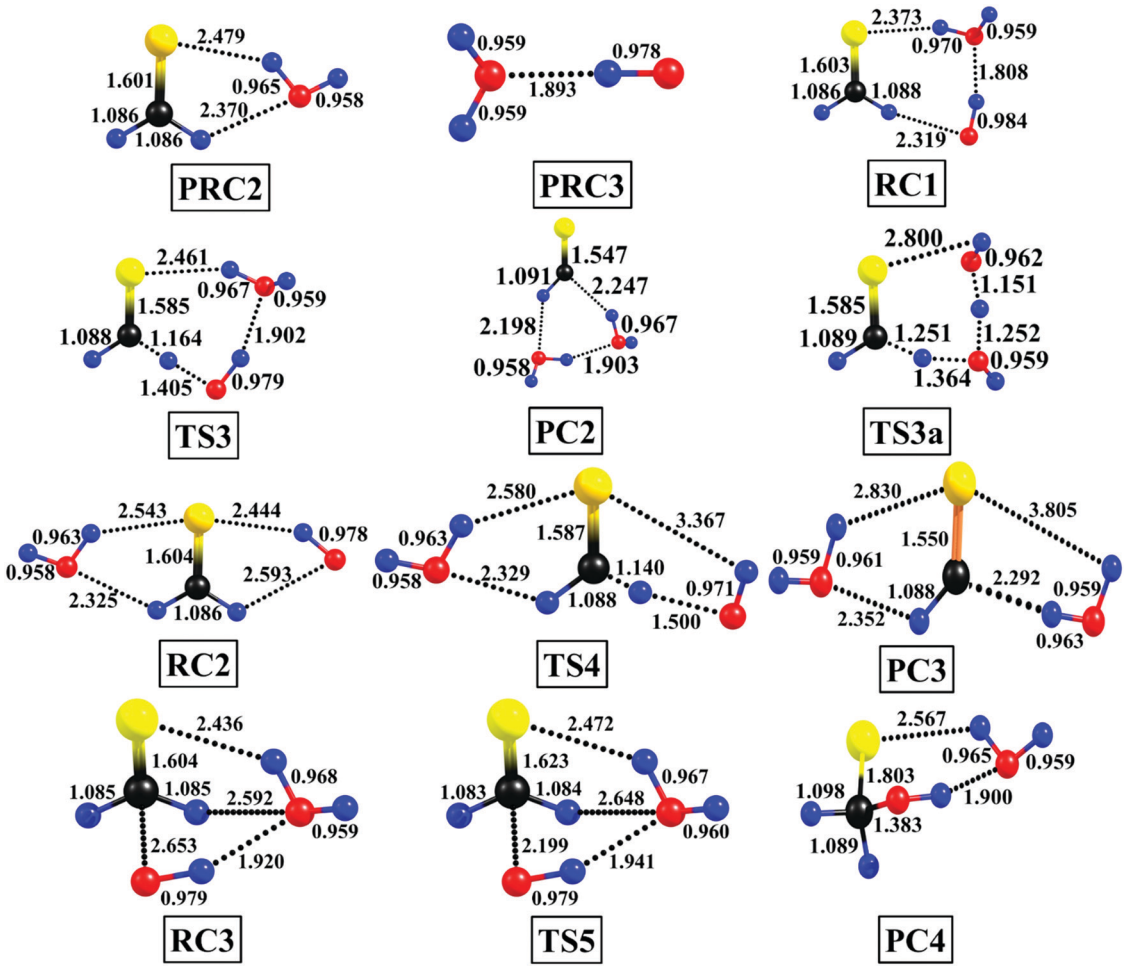

Fig. 4 Optimized geometries of the dimer complexes (PRCs), reactant complexes (RCs), transition states (TSs), and product complexes (PCs) for the H_2CS + $^{\bullet}OH$ reaction assisted by a single water molecule obtained at the M06-2X/6-311++G(3df,3pd) level of theory. The yellow, black, and blue colors denote sulfur, carbon, and hydrogen atoms, respectively.

relative to the energy of the starting reactants, to form product complex PC3. This indicates that TS4 lies 3.0 kcal mol^{-1} above the energy of TS3. As a result, the reaction channel through RC2 and TS4 will not be competitive compared with that of the reaction channel through RC1 and TS3 at normal atmospheric temperatures.

From Fig. 3, it can be concluded that for the hydrogen abstraction reaction of H_2CS + $^{\bullet}OH$ catalyzed by H_2O, the reaction channel through $OH\cdots H_2O$ + H_2CS should be more dominant due to the larger binding energy of the dimer complex compared to other possible channels. Therefore, the $OH\cdots H_2O$ + H_2CS reaction *via* RC1, TS3, and PC2 to form $H^{\bullet}CS$ + $2H_2O$ as final products, will be the major channel. The remaining $H_2CS\cdots OH$ + H_2O and $H_2CS\cdots H_2O$ + $^{\bullet}OH$ reaction channels may be significant only at higher concentrations of H_2CS in the atmosphere.

We also performed calculations on OH radical addition to the sp^2 C-atom of H_2CS in the presence of a single water molecule. Similar to the water assisted H-abstraction pathways (5a)–(5c), the addition reaction also proceeds by forming dimer complexes from the three reagents H_2CS, $^{\bullet}OH$, and H_2O. The formed dimer complexes then collide with the other remaining reactant through the bimolecular encounters shown in eqn (6a) and (6b):

$$H_2CS\cdots H_2O + {}^{\bullet}OH \rightarrow H_2C(OH)S^{\bullet} + H_2O \quad (6a)$$

$$H_2CS + OH\cdots H_2O \rightarrow H_2C(OH)S^{\bullet} + H_2O \quad (6b)$$

The PESs involving various stationary points for the addition of OH radical to the C-atom of H_2CS assisted by a single H_2O molecule are also shown in Fig. 3. Similar to the abstraction channel, the addition pathway also proceeds *via* dimer complexes that collide with the isolated monomer reactant shown in the entrance channels in Fig. 3. This results in a reactant complex (RC3) with a binding energy of 7.2 kcal mol^{-1} below that of the separated reactants, which then passes through a transition state (TS5) with a barrier height of −6.7 kcal mol^{-1} relative to that of the separated H_2CS + $^{\bullet}OH$ + H_2O reagents. This value suggests that the $^{\bullet}OH$ addition pathway has a ~6 kcal mol^{-1} lower barrier compared to the H_2CS + $^{\bullet}OH$ reaction in the absence of water. The formed TS5 then proceeds *via* a product complex (PC4) to form the final products

(OH)$CH_2S^{\bullet}$ + H_2O. The barrier height for this reaction is 1.2 kcal mol^{-1} lower compared to the barrier for the abstraction channel (TS3). Therefore, based on the energetics of the various possible reactions involved in the H_2CS + $^{\bullet}OH$ + H_2O reaction, the addition channel will be the more dominant reaction when compared to the abstraction channel.

The concentration of water dimer present in the atmosphere is $\sim 9 \times 10^{14}$ molecule cm^{-3} at 298 K.[61] Various studies have reported that the water dimer also plays an important role in H-atom abstraction reactions.[62–64] Therefore, as an example, we only investigated the H-atom abstraction channel for the H_2CS + $^{\bullet}OH$ reaction catalyzed by the water dimer in order to compare the results to those observed with the uncatalyzed and water catalyzed channels. The H_2CS + $^{\bullet}OH$ reaction catalyzed by the water dimer proceeds by the following reaction pathways (7) and (8).

$$^{\bullet}OH\cdots(H_2O)_2 + H_2CS \rightarrow H^{\bullet}CS + 3H_2O \quad (7)$$

$$H_2CS\cdots(H_2O)_2 + {}^{\bullet}OH \rightarrow H^{\bullet}CS + 3H_2O \quad (8)$$

In the presence of the water dimer both H_2CS and $^{\bullet}OH$ interact *via* hydrogen bonding to form the corresponding trimer complexes $^{\bullet}OH\cdots(H_2O)_2$ (PRC4), and $H_2CS\cdots(H_2O)_2$ (PRC5) at the entrance channels on the PES shown in Fig. 5. The energies for all the minima with respect to the starting reactants on the PES were calculated at the CCSD(T)//M06-2X level. The optimized geometries for all the stationary points on the PES are given in Fig. S1 (ESI†). The formed PRC4 and PRC5 collide with the other isolated reactant (*i.e.* PRC4 + H_2CS and PRC5 + $^{\bullet}OH$) to form their corresponding reactant complexes RC4 and RC5, with binding energies of −14.1 and −13.5 kcal mol^{-1}, respectively. The reaction proceeds from RC4 *via* the formation of transition state (TS6) with a barrier height of −12.2 kcal mol^{-1} relative to the starting reagents. This then proceeds to form product complex (PC5) and then to the formation of $H^{\bullet}CS$ + $3H_2O$ as separated products. This barrier height value suggests that the water dimer reduces the barrier for the H-atom abstraction channel by ∼12.4 and ∼6.7 kcal mol^{-1} compared to the values for the uncatalyzed and water catalyzed reactions respectively. An alternative transition state (TS7) was also found for this reaction with a barrier height of −0.8 kcal mol^{-1} relative to the separated reactants. In TS7, the position of the OH radical is interchanged when compared to the arrangement observed in TS6 (see Fig. S1, ESI†). We did not consider this alternative transition state arrangement (*i.e.* TS7) in the kinetic calculations because it has a ∼11.4 kcal mol^{-1} higher barrier compared to transition state TS6. The other H-abstraction channel was also found to proceed *via* the bimolecular collision between PRC5 and $^{\bullet}OH$ by forming a reactant complex RC6, with a binding energy of −12.3 kcal mol^{-1}. The $^{\bullet}OH$ and water dimer in RC6 are separated from each other, whereas in RC4 and RC5, both OH and the water dimer are held together in a ring-like configuration. The reaction then continues *via* transition state TS8 with a barrier height of −8.2 kcal mol^{-1} relative to the separated reactants. TS8 leads to the formation of PC7 and then to the same $H^{\bullet}CS$ + $3H_2O$ separated products (see Fig. 5). The barrier height *via* TS8 for this reaction is also ∼4 kcal mol^{-1} higher compared to the value of TS6. Therefore, we did not consider the transition state TS8 in the rate constant calculations.

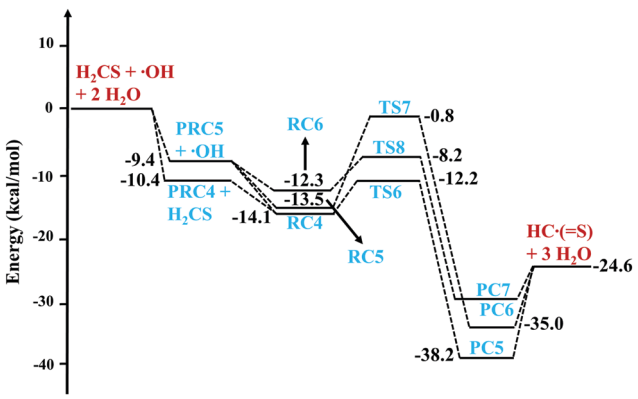

Fig. 5 Potential energy surface diagram for the H-atom abstraction channel involving the H_2CS + $^{\bullet}OH$ reaction assisted by the water dimer obtained at the CCSD(T)/aug-cc-pVTZ//M06-2X/6-311++G(3df,3pd) level. PRC4 and PRC5 correspond to the $HO\cdots(H_2O)_2$ and $H_2CS\cdots(H_2O)_2$ trimers respectively, RC4, RC5, RC6 denote reactant complexes, TS6, TS7, TS8 correspond to transition states, and PC5, PC6, PC7 refer to product complexes.

3.2. Theoretical kinetic analysis

We performed rate constant calculations using the energies obtained from the aforementioned electronic structure calculations, to determine the potential impact of a single water molecule as a catalyst on the H_2CS + $^{\bullet}OH$ reaction. Here, we followed a procedure analogous to that reported in several previously published articles.[36–40,48] As mentioned earlier, the bimolecular reactions associated with the H_2CS + $^{\bullet}OH$ + H_2O reaction occur through a dimer (R1) that reacts by colliding with a monomer (R2) leading to the formation of a barrierless RC. The formed RC then undergoes unimolecular isomerization to form final products (eqn (9)):

$$R1 + R2 \underset{k_{-1}}{\overset{k_1}{\rightleftharpoons}} RC \xrightarrow{k_2} \text{Products} \quad (9)$$

In eqn (9), R1, R2, and RC represent a two body complex (reactant-1), isolated monomer (reactant-2), and a reactant complex, respectively. The rate constants k_1 and k_{-1} are the forward and reverse rate constants for the formation of RC from the reactants R1 and R2, and the rate constant k_2 corresponds to the product formation step. A steady-state analysis leads to a rate constant for the overall reaction (eqn (10)) that can be defined as:

$$k = \frac{k_1 k_2}{k_{-1} + k_2} \quad (10)$$

Although the energy barrier for the k_{-1} and k_2 are comparable, the rate constant k_{-1} is considerably larger than that of k_2 (*i.e.* $k_{-1} \gg k_2$), because the entropy change is much larger in the reverse reaction due to its very loose transition state for this reaction step compared to that for the formation of the

products. With this assumption, the overall bimolecular rate constant (k) can be given as eqn (11), which is derived by assuming the reactant complex (RC) is in equilibrium with reactants and that RC exists under steady state conditions.

$$k = \left(\frac{k_1}{k_{-1}}\right)k_2 = K_{eq}^{RC}k_2 \quad (11)$$

In eqn (11), the equilibrium constant (K_{eq}^{RC}) represents the formation of a reactant complex (RC) from the two reactants (R1 (dimer) and R2 (monomer)) shown in the first step of eqn (9). The temperature dependent equilibrium constant (K_{eq}^{RC}) value was calculated using partition functions associated with R1, R2, and RC. The partition functions of these species were calculated using basic equations from statistical mechanics.[65] For the calculations, the required vibrational frequencies and rotational constants were computed at the M06-2X/6-311++G(3df,3pd) level of theory. The association of the two reactants (R1 and R2) to form RC at the entrance channel is a barrierless reaction. The TS for this reaction step is not fixed and varies with energy along the reaction coordinate. Therefore, we used the equilibrium approach to account for the presence of the forward and backward reactions. The rate constants calculated using this kinetic model are reasonably correct under high pressure limit conditions. This kinetic approach using the single TS model has been applied by various research groups for water catalyzed reactions.[36,38,40,66,67] The obtained rate constants using this kinetic method are in very good agreement with the experimentally measured values.[67] The rate constants were reported for the water catalyzed CH_3CHO + $^{\bullet}OH$, H_2CO + $^{\bullet}OH$, CH_2CH_2 + $^{\bullet}OH$, and CH_2NH + $^{\bullet}OH$ reactions using the present kinetic model, and the results with the single transition approach are in good agreement with theoretically calculated and experimentally measured values.[38,40,67] Ali and Barker also studied the H_2CO + $^{\bullet}OH$ reaction using the two TS model, and the rate constants were compared with the single-TS model for the same reaction.[60,66] The reported rate constants using both approaches were in reasonably good agreement with each other (within a factor of $\sim$2 at 298 K).[60,66] Based on these studies, we used the single TS approach in the rate constant calculation for the H_2CS + $^{\bullet}OH$ reaction assisted by a water molecule, and we believe it to be accurate based on the aforementioned considerations. In addition to these calculations, the unimolecular rate constant (k_2) was calculated using the canonical variational transition state theory (CVT)[42,43] with the small curvature tunneling (SCT) method[41] developed in Polyrate (2016)[68] (presented in eqn (12) below):

$$k_2(\mathrm{CVT/SCT}) = \kappa^{SCT}\frac{k_B T}{h}\frac{Q_{GT}(s^*)}{Q_{RC}}e^{\frac{-V(S^*)}{k_B T}} \quad (12)$$

In eqn (12), κ^{SCT} is the SCT parameter, s^* is the value of the reaction coordinate at the free energy maximum along the reaction path, k_B is Boltzmann's constant, h is Planck's constant, $V(s^*)$ is the potential energy at the barrier maximum, Q_{RC} and $Q_{GT}(s^*)$ are the partition functions of the reactant complex and transition state, respectively, and T is the temperature in Kelvin.

The forward isomerization barrier for RC3 is only 0.5 kcal mol^{-1} (see Fig. 3). However, the reaction scheme and kinetic model employed in this work for the rate constant calculation using RC3 is still valid, because the transition state (TS5) formed through RC3 lies $\sim$5.7 kcal mol^{-1} and $\sim$8.1 kcal mol^{-1} higher in terms of free energy, relative to the $H_2CS\cdots H_2O$ + $^{\bullet}OH$ and $OH\cdots H_2O$ + H_2CS separated reactants respectively. Therefore, this reaction scheme and kinetic approach is valid for the reaction involving RC3.

As discussed in the previous section, the H_2CS + $^{\bullet}OH$ + H_2O reaction proceeds *via* a dimer complex that collides with the left-out monomer reactant. As an example, the H_2CS + $^{\bullet}OH$ + H_2O reaction can proceed in principle through four possible reaction paths (two each for addition and abstraction pathways) including $H_2CS\cdots H_2O$ + $^{\bullet}OH$, and H_2CS + $HO\cdots H_2O$ as illustrated in reactions (5a), (5b) and (6a), (6b). These reaction pathways lead to the formation of a RC, which is in equilibrium with the reactants. This RC then undergoes unimolecular isomerization by passing through a TS to form the corresponding products (shown in eqn (9)). The calculation of the equilibrium constant (K_{eq}^{RC}) for reactant complex formation from the reaction of a dimer complex and a monomer can be accomplished using eqn (13).

$$K_{eq}^{RC} = \frac{Q_{RC}}{Q_{R1}Q_{R2}}\exp\left(-\frac{E_{RC}-E_R}{k_B T}\right) \quad (13)$$

In eqn (13), the partition functions of a RC formed from the corresponding dimer complex (reactant-1) and monomer (reactant-2) are labelled Q_{RC}, Q_{R1}, and Q_{R2} respectively. E_R and E_{RC} are the zero-point corrected total energies of the reactants and reactant complex respectively, computed at the CCSD(T)//M06-2X level. The bimolecular rate constants (in units of cm^3 molecule^{-1} s^{-1}) for the $H_2CS\cdots H_2O$ + $^{\bullet}OH$ and H_2CS + $HO\cdots H_2O$ reaction paths through eqn (5a), (5b) and (6a), (6b) were calculated using the expressions: $k_{5a} = K_{eq1}k_2$, $k_{5b} = K_{eq2}k_2$, $k_{6a} = K_{eq1}k_3$, and $k_{6b} = K_{eq2}k_3$, respectively and are provided in Tables S12–S14 (ESI†). In these expressions, the equilibrium constants K_{eq1} and K_{eq2} are associated with the reaction of a dimer and monomer combination to form the corresponding RC. The temperature dependent unimolecular rate constants (k_2 and k_3 are in s^{-1}) and the bimolecular rate constants (k_n (n = 5a, 5b, 6a, and 6b) in cm^3 molecule^{-1} s^{-1}) calculated using the CVT/SCT method at temperatures between 200 and 400 K are displayed in Tables S13 and S14 (ESI†) for the two possible reaction paths. The total bimolecular rate constant (cm^3 molecule^{-1} s^{-1}) for the addition reaction of H_2CS + $^{\bullet}OH$ + H_2O is $\sim$3 to $\sim$9 times smaller than that of the abstraction reaction in the temperature range from 200 to 250 K, and above this temperature ($>$260 K) were found to be $\sim$1 order of magnitude smaller. For example, the overall bimolecular rate constants for the addition and abstraction reactions at 300 K were calculated to be 5.8×10^{-11} cm^3 molecule^{-1} s^{-1} and 9.7×10^{-10} cm^3 molecule^{-1} s^{-1}, respectively. The distinction between the two is a consequence mainly of the following important differences between the addition and abstraction

reactions: (1) the equilibrium constants involved in RC1 formation (abstraction reaction) from the dimers and the isolated reactant, are larger by ~3 orders of magnitude at 300 K, compared to the equilibrium constants involved in the formation of RC3 (addition reaction). For example, the equilibrium constant involved in the formation of RC3 (addition path), and RC1 (abstraction reaction) from the $H_2CS + OH\cdots H_2O$ reaction was calculated to be 6.4×10^{-23} cm^3 $molecule^{-1}$ and 9.6×10^{-20} cm^3 $molecule^{-1}$ respectively at 300 K; (2) the CVT/SCT calculated unimolecular rate constant for the addition reaction was found to be ~2 orders of magnitude higher than for the abstraction reaction. For example, at 300 K, the unimolecular rate constants for the addition and abstraction reactions were calculated to be 5.4×10^{11} s^{-1} and 6.0×10^{9} s^{-1}, respectively. Therefore, the resultant bimolecular rate constant for the addition reaction is ~1 order of magnitude smaller than that for the abstraction reaction. In addition, the tunneling contributions calculated using the SCT method were included in the rate constants for both the addition and abstraction reactions, and the values are displayed in Table S15 (ESI†). The data from the table show that between 200–250 K, the rate constants are increased by ~2–3 times due to tunneling. Beyond these temperatures, tunneling was found to be insignificant.

Based on the calculated energy results, the reaction of OH radical with H_2CS molecules is also an important atmospheric removal process. Therefore, we performed rate constant calculations for the $H_2CS + {}^{\bullet}OH$ reaction without water through eqn (1) and (2) using the CVT/SCT method at the atmospherically relevant temperature range between 200 and 400 K, to compare it with that of the $H_2CS + {}^{\bullet}OH + H_2O$ reaction. The unimolecular rate constants (s^{-1}), equilibrium constants (K_{eq}), and bimolecular rate constants (cm^3 $molcule^{-1}$ s^{-1}) for the $H_2CS + {}^{\bullet}OH$ reaction were calculated for both reaction pathways 1 and 2 and the values are displayed in Tables S12 and S16 (ESI†). The data from Table S16 (ESI†) suggest that the addition reaction rate constants are ~3–8 times larger than those for the abstraction reactions. These results are also consistent with barrier heights for the abstraction reaction which were found to be ~1.0 kcal mol^{-1} higher than for the addition channel. For example, the bimolecular rate constant for the $H_2CS + {}^{\bullet}OH$ addition and abstraction reactions at 300 K were found to be 4.9×10^{-12} cm^3 $molecule^{-1}$ s^{-1} and 1.5×10^{-12} cm^3 $molecule^{-1}$ s^{-1}, respectively.

The total bimolecular rate constants ($k_{OH} = k_{R1} + k_{R2}$) for the $H_2CS + {}^{\bullet}OH$ reaction given in Table S16 (ESI†) were compared with the values of previously reported isoelectronic systems.[60] The total bimolecular rate constant for the $H_2CS + {}^{\bullet}OH$ reaction was found to be 6.41×10^{-12} cm^3 $molecule^{-1}$ s^{-1} at 300 K, and the values reported by Ali and Barker[60] for the $H_2CO + {}^{\bullet}OH$, $H_2CNH + {}^{\bullet}OH$, and $CH_2CH_2 + {}^{\bullet}OH$ reaction systems were 5.77×10^{-12} cm^3 $molecule^{-1}$ s^{-1}, 4.00×10^{-12} cm^3 $molecule^{-1}$ s^{-1}, and 5.76×10^{-12} cm^3 $molecule^{-1}$ s^{-1}, respectively at the same temperature. These data suggest that the $H_2CS + {}^{\bullet}OH$ reaction rate constant agrees well with the values of the other three isoelectronic systems.

We also calculated the atmospheric life time of H_2CS with respect to its reaction with OH radical, using the formula[33] $\tau = 1/k_{OH}[OH]$, where k_{OH} represents the total bimolecular rate constant for the $H_2CS + {}^{\bullet}OH$ reaction and [OH] is the average concentration of the OH radical (~1.0×10^6 molecules cm^{-3}) in the atmosphere.[33] The atmospheric lifetime of H_2CS in the atmospherically relevant temperatures between 200–400 K is estimated to be 1–2 days. These values were calculated by using the total bimolecular rate constants given in Table S16 (ESI†) and the average concentration of OH radical in the atmosphere.

The addition and abstraction reaction rate constants were compared for the $H_2CS + {}^{\bullet}OH$ reaction in the presence and absence of water in the temperatures between 200 and 400 K, and are shown in Fig. 6. The data suggest that the rate constants for the OH addition to the sp^2 carbon atom to form $H_2C(OH)S^{\bullet} + H_2O$ are ~2–8 times higher than those for the H atom abstraction reaction in the studied temperature range. This is primarily because the barrier height of the OH addition is ~1.0 kcal mol^{-1} lower than that for the H atom abstraction path. The bimolecular rate constants for the water catalyzed reactions (5a), (5b) and (6a), (6b) were calculated in the same temperature range. The total effective bimolecular rate constant data for the abstraction (k^{eff}_{total}) and addition (k^{eff}_{total}) reactions were calculated and plotted in the same figure and the values are displayed in Tables S13 and S14 (ESI†). The results suggest that the total effective bimolecular rate constants for the abstraction reaction are ~1–2 orders of magnitude higher than for the addition reaction. For example, at 300 K, the total bimolecular abstraction and addition reaction rate constants were found to be 2.0×10^{-14} cm^3 $molecule^{-1}$ s^{-1}

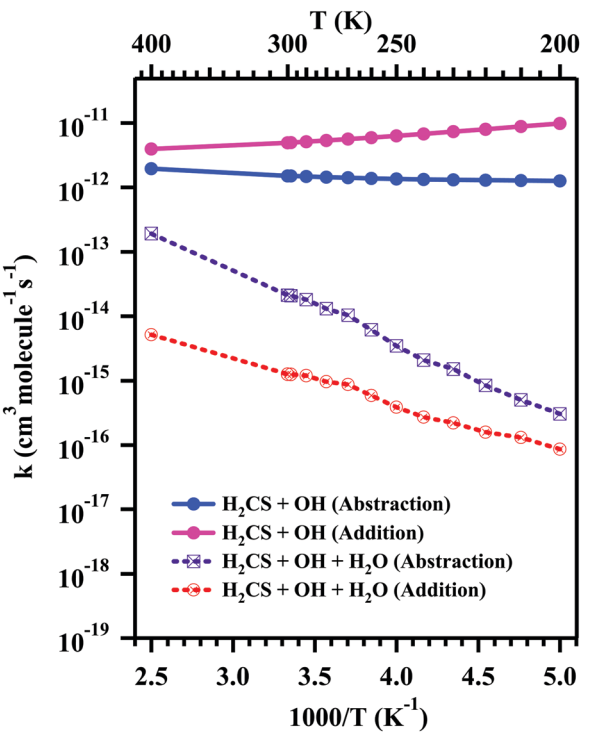

Fig. 6 The calculated rate constants (in cm^3 $molcule^{-1}$ s^{-1}) for the $H_2CS + {}^{\bullet}OH$ reaction in the presence and absence of water in the temperatures between 200 and 400 K.

and 1.3×10^{-15} cm^3 molecule^{-1} s^{-1}, respectively. Thus, the rate constant data in Fig. 6 and Tables S13, S14 and S16 (ESI†) suggest that the addition reaction is ~2–9 times more dominanant than the abstraction path in the absence of water. Conversely, in the water assisted reaction, the abstraction channel is ~3–37 times more dominant than the addition channel.

To determine the potential impact of a single water molecule on the $H_2CS + {}^{\bullet}OH$ reaction in comparison with that of the same reaction in the absence of the catalyst, it is essential to compare the rates of these two reactions. We estimated the corresponding effective first order rate constants (s^{-1}) for both $H_2CS + {}^{\bullet}OH + H_2O$ and $H_2CS + {}^{\bullet}OH$ reactions using the approach outlined below. For example, the rate for the $H_2CS\cdots H_2O + {}^{\bullet}OH$ reaction can be written as:

$$\nu_{5a} = k_{5a}[H_2CS\cdots H_2O][{}^{\bullet}OH] \quad (14)$$

In eqn (14), the $H_2CS\cdots H_2O$ dimer (PRC2) concentration can be written in terms of the corresponding isolated reactant concentrations, and the dimer formation step equilibrium constant κ_{eq2} is given as:

$$\nu_{5a} = k_{5a}\kappa_{eq2}[H_2O][{}^{\bullet}OH][H_2CS] \quad (15)$$

In eqn (15), combining the first four terms (*i.e.* $k_{5a}\kappa_{eq2}[H_2O][{}^{\bullet}OH]$), the rate can be written in terms of the effective first order rate constant (k_{5a}^{eff}) for the atmospheric removal of H_2CS molecules, as given in eqn (16).

$$\nu_{5a} = k_{5a}^{eff}[H_2CS] \quad (16)$$

Using a similar approach for the other possible elementary reactions of the $H_2CS + {}^{\bullet}OH + H_2O$ and $H_2CS + {}^{\bullet}OH$ pathways through eqn (5b), (6a), (6b) and (1), (2), gives:

$$\nu_{5b} = k_{5b}[H_2O\cdots OH][H_2CS] = k_{5b}\kappa_{eq3}[H_2O][{}^{\bullet}OH][H_2CS] = k_{5b}^{eff}[H_2CS] \quad (17)$$

$$\nu_{6a} = k_{6a}[H_2CS\cdots H_2O][{}^{\bullet}OH] = k_{6a}\kappa_{eq2}[H_2O][{}^{\bullet}OH][H_2CS] = k_{6a}^{eff}[H_2CS] \quad (18)$$

$$\nu_{6b} = k_{6b}[H_2O\cdots OH][H_2CS] = k_{6b}\kappa_{eq3}[H_2O][{}^{\bullet}OH][H_2CS] = k_{6b}^{eff}[H_2CS] \quad (19)$$

$$\nu_1 = k_1[H_2CS][{}^{\bullet}OH] = k_1^{eff}[H_2CS] \quad (20)$$

$$\nu_2 = k_2[H_2CS][{}^{\bullet}OH] = k_2^{eff}[H_2CS] \quad (21)$$

The equilibrium constants (κ_{eq2}, and κ_{eq3}) for the formation of dimers such as $H_2CS\cdots H_2O$ and $H_2O\cdots OH$ respectively, are given in Table S12 of the ESI.† The effective first order rate constants for the addition and abstraction channels involving $H_2CS\cdots H_2O + {}^{\bullet}OH$, $H_2O\cdots OH + H_2CS$, and $H_2CS + {}^{\bullet}OH$ reactions were calculated using the expressions given in eqn (16)–(21). The total effective first order rate constant for the abstraction (k_{abs}^{eff}) and addition (k_{add}^{eff}) pathways through $H_2CS\cdots H_2O + {}^{\bullet}OH$ and $OH\cdots H_2O + H_2CS$ reactions were calculated using eqn (22) and (23).

$$k_{abs}^{eff}(H_2CS + {}^{\bullet}OH + H_2O) = k_{5a}^{eff} + k_{5b}^{eff} \quad (22)$$

$$k_{add}^{eff}(H_2CS + {}^{\bullet}OH + H_2O) = k_{6a}^{eff} + k_{5b}^{eff} \quad (23)$$

Then the total effective first order rate constant (k_{total}^{eff}) for the overall reaction was calculated by summing the individual effective first order rate constants for each reaction pathway for both $H_2CS + {}^{\bullet}OH + H_2O$ and $H_2CS + {}^{\bullet}OH$ reactions (presented below):

$$k_{total}^{eff}(H_2CS + {}^{\bullet}OH + H_2O) = k_{5a}^{eff} + k_{5b}^{eff} + k_{6a}^{eff} + k_{6b}^{eff} \quad (24)$$

$$k_{total}^{eff}(H_2CS + {}^{\bullet}OH) = k_1^{eff} + k_2^{eff} \quad (25)$$

Using eqn (22)–(25), the total effective rate constants for the addition and abstraction channels, and the total effective first order rate constants (in s^{-1}) for the $H_2CS + {}^{\bullet}OH + H_2O$ and $H_2CS + {}^{\bullet}OH$ reactions were calculated in the temperature range of 200–400 K, and the values are displayed in Tables 1 and 2. The effective rate constant values in Tables 1 and 2 were generated by using the average atmospheric concentration of OH ([OH] = 1×10^6 molecule cm^{-3}), and the water concentration at the corresponding temperature. The temperature dependent water concentrations from 200 to 400 K are given in Table 2, and were calculated based on using a typical water concentration, which corresponds to 10–100% relative humidity.[38] These water concentrations were taken from ground level to higher altitudes (typically between the 0–15 km range) in the atmosphere. The concentration of [H_2O] decreases with increasing altitude. The rate data from Table 2 suggest that the H-atom abstraction and addition channels involving the $H_2CS\cdots H_2O + {}^{\bullet}OH$ reaction are ~2 times higher than the values for the $OH\cdots H_2O + H_2CS$ reaction pathway. The total effective first order rate constant for the abstraction channel (k_{abs}^{eff}) involving the $H_2CS + {}^{\bullet}OH + H_2O$ reaction is ~3–35 times higher than the addition channel rate constant (k_{add}^{eff}) in the studied temperature range. We have also compared the effective rate constants for the abstraction and addition channels involving the $H_2CS + {}^{\bullet}OH + H_2O$ and $H_2CS + {}^{\bullet}OH$ reactions. The effective rate constants for the abstraction channel involving the $H_2CS + {}^{\bullet}OH$ reaction assisted by water is ~1–3 orders of magnitude lower than in the absence of a catalyst. As in the case of the addition channel, the $H_2CS + {}^{\bullet}OH$ reaction assisted by water is

Table 1 The effective first order rate constants (k_n^{eff} (n = 1, 2, total) in s^{-1}) for the gas phase reaction of $H_2CS + {}^{\bullet}OH$ over the temperatures between 200 and 300 K

T (K)	k_1^{eff}	k_2^{eff}	$k_{total}^{eff} = k_1^{eff} + k_2^{eff}$
200	1.26×10^{-6}	9.82×10^{-6}	1.11×10^{-5}
210	1.27×10^{-6}	8.80×10^{-6}	1.01×10^{-5}
220	1.29×10^{-6}	7.98×10^{-6}	9.27×10^{-6}
230	1.31×10^{-6}	7.32×10^{-6}	8.62×10^{-6}
240	1.32×10^{-6}	6.77×10^{-6}	8.09×10^{-6}
250	1.35×10^{-6}	6.32×10^{-6}	7.67×10^{-6}
260	1.38×10^{-6}	5.93×10^{-6}	7.31×10^{-6}
270	1.41×10^{-6}	5.61×10^{-6}	7.02×10^{-6}
280	1.44×10^{-6}	5.34×10^{-6}	6.78×10^{-6}
290	1.47×10^{-6}	5.11×10^{-6}	6.58×10^{-6}
298	1.50×10^{-6}	4.94×10^{-6}	6.45×10^{-6}
300	1.50×10^{-6}	4.91×10^{-6}	6.41×10^{-6}
400	1.94×10^{-6}	3.95×10^{-6}	5.90×10^{-6}

Table 2 The effective reaction rate constants (k_{eff} in s^{-1}) for the $H_2CS\cdots H_2O$ + •OH and $OH\cdots H_2O$ + H_2CS reaction paths involved in the H_2CS + H_2O + •OH reaction in the temperature range between 200 and 300 K

		Abstraction channels			Addition channels			
T (K)	$[H_2O\cdots H_2O]^a$ (molecule cm^{-3})	$H_2CS\cdots H_2O$ + •OH (k_{5a}^{eff})	$OH\cdots H_2O$ + H_2CS (k_{5b}^{eff})	$k_{abs}^{eff} = k_{5a}^{eff} + k_{5b}^{eff}$	$H_2CS\cdots H_2O$ + •OH (k_{6a}^{eff})	$OH\cdots H_2O$ + H_2CS (k_{6b}^{eff})	$k_{add}^{eff} = k_{6a}^{eff} + k_{6b}^{eff}$	$k_{total}^{eff} = k_{5a}^{eff} + k_{5b}^{ef} + k_{6a}^{efff} + k_{6b}^{eff}$
200	1.09×10^{14}	2.03×10^{-10}	1.01×10^{-10}	3.04×10^{-10}	5.73×10^{-11}	2.86×10^{-11}	8.59×10^{-11}	3.90×10^{-10}
210	6.00×10^{14}	5.56×10^{-10}	2.66×10^{-10}	8.21×10^{-10}	1.26×10^{-10}	6.29×10^{-11}	1.89×10^{-10}	1.01×10^{-9}
220	1.15×10^{15}	5.70×10^{-10}	2.73×10^{-10}	8.42×10^{-10}	1.05×10^{-10}	5.26×10^{-11}	1.58×10^{-10}	1.00×10^{-9}
230	5.80×10^{15}	1.63×10^{-9}	7.82×10^{-10}	2.41×10^{-9}	2.50×10^{-10}	1.25×10^{-10}	3.75×10^{-10}	2.78×10^{-9}
240	8.29×10^{15}	1.40×10^{-9}	6.71×10^{-10}	2.07×10^{-9}	1.80×10^{-10}	9.01×10^{-11}	2.70×10^{-10}	2.34×10^{-9}
250	2.21×10^{16}	2.32×10^{-9}	1.12×10^{-9}	3.43×10^{-9}	1.57×10^{-10}	1.28×10^{-10}	3.85×10^{-10}	3.82×10^{-9}
260	6.00×10^{16}	4.13×10^{-9}	1.99×10^{-9}	6.12×10^{-9}	3.93×10^{-10}	1.96×10^{-10}	5.89×10^{-10}	6.70×10^{-9}
270	1.50×10^{17}	6.97×10^{-9}	3.37×10^{-9}	1.03×10^{-8}	5.80×10^{-10}	2.90×10^{-10}	8.71×10^{-10}	1.12×10^{-8}
280	2.70×10^{17}	8.77×10^{-9}	4.24×10^{-9}	1.30×10^{-8}	6.43×10^{-10}	3.22×10^{-10}	9.65×10^{-10}	1.40×10^{-8}
290	5.20×10^{17}	1.22×10^{-8}	5.88×10^{-9}	1.80×10^{-8}	7.92×10^{-10}	3.96×10^{-10}	1.19×10^{-9}	1.92×10^{-8}
298	7.64×10^{17}	1.39×10^{-8}	6.75×10^{-9}	2.07×10^{-8}	8.29×10^{-10}	4.15×10^{-10}	1.24×10^{-9}	2.19×10^{-8}
300	8.24×10^{17}	1.42×10^{-8}	6.90×10^{-9}	2.11×10^{-8}	8.31×10^{-10}	4.15×10^{-10}	1.25×10^{-9}	2.24×10^{-8}
400	5.72×10^{19}	1.29×10^{-7}	6.29×10^{-8}	1.92×10^{-7}	3.41×10^{-9}	1.70×10^{-9}	5.11×10^{-9}	1.97×10^{-7}

[a] Values of water concentration calculated based on using a typical temperature-dependent water concentration, which corresponds to 10%–100% relative humidity.

~2–5 orders of magnitude lower than for the H_2CS + •OH reaction in the absence of a catalyst.

The total effective first order rate constants for the H_2CS + •OH + H_2O and H_2CS + •OH reactions were compared at the atmospherically relevant temperatures between 200 and 400 K as shown in Fig. 7. The trends in Fig. 7 suggest that the effective first order rate constants increase linearly with temperature in the case of H_2CS + •OH + H_2O, and in the case of the H_2CS + •OH reaction, they were found to be almost independent of temperature.

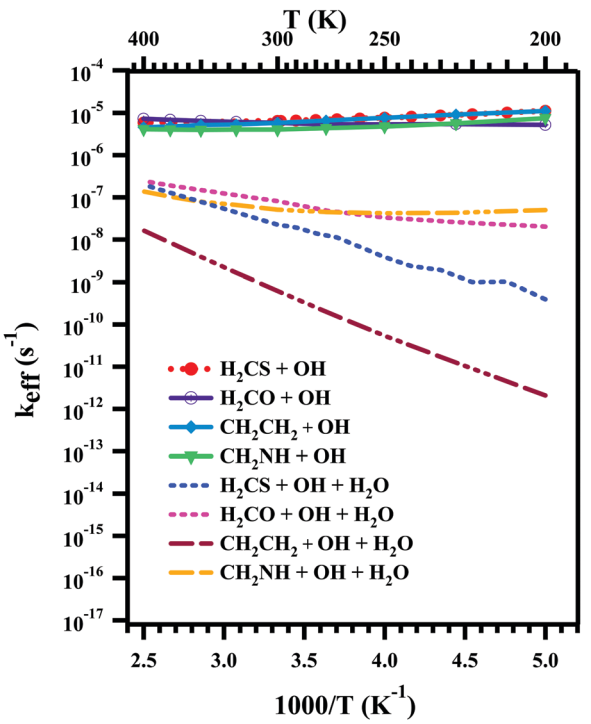

Fig. 7 Comparison of the effective reaction rate constants (k_{eff} in s^{-1}) in the absence and presence of water for four isoelectronic reaction systems: H_2CS + •OH, CH_2O + •OH, CH_2CH_2 + •OH, and CH_2NH + •OH in the temperature range between 200–400 K.

It is apparent that the H_2CS + •OH reaction is faster than the H_2CS + •OH + H_2O reaction by about ~1–4 orders of magnitude in the studied temperatures between 200 and 400 K. For example, at 300 K, the effective first order rate constant for the H_2CS + •OH + H_2O and H_2CS + •OH reactions were 2.2×10^{-8} s^{-1} and 6.4×10^{-6} s^{-1}, respectively.

The total effective first order rate constants for H_2CS + •OH, and the same reaction assisted by a single water molecule, were also compared with the previously reported values[38,60] for the three isoelectronic reaction systems H_2CO + •OH, CH_2CH_2 + •OH, and CH_2NH + •OH, both in the absence and presence of a single water molecule in the temperatures between 200 and 400 K. The results are plotted in Fig. 7. For comparison with the H_2CS + •OH reaction, the total effective first order rate constant (s^{-1}) data in Fig. 7 were generated by multiplying the [OH] = 1.0×10^6 molecules cm^{-3} with the previously reported total bimolecular[60] rate constant (cm^3 $molecule^{-1}$ s^{-1}) and total effective bimolecular rate constants[38] (cm^3 $molecule^{-1}$ s^{-1}) for H_2CO + •OH, CH_2CH_2 + •OH, and CH_2NH + •OH, with and without a single water molecule. The results in Fig. 7 suggest that the total effective first order rate constant for the H_2CS + •OH reaction is in excellent agreement with the corresponding values for the H_2CO + •OH, CH_2CH_2 + •OH, and CH_2NH + •OH reactions in the studied temperature range. However, the H_2CS + •OH + H_2O total effective first order rate constants are ~1 order of magnitude higher than the values for the CH_2NH + •OH + H_2O and H_2CO + •OH + H_2O reactions in the temperatures between 200 and 250 K. Above this temperature (>250 K) these values become ~2–4 times smaller. In addition, the total effective first order rate constants for H_2CS + •OH + H_2O were also compared with the CH_2CH_2 + •OH + H_2O reaction in the same temperature range. Fig. 7 clearly shows that the effective first order rate constant values are ~1–2 orders of magnitude larger than the values for the CH_2CH_2 + •OH + H_2O reaction at temperatures between 200 and 400 K. The large difference in the effective rate constant values between the H_2CS + •OH + H_2O and CH_2CH_2 + •OH + H_2O reactions in the studied temperature range is due to the

fact that the single water molecule did not decrease the barrier heights in the CH_2CH_2 + $^{\bullet}OH$ reaction compared to the H_2CS + $^{\bullet}OH$ reaction at atmospherically relevant temperatures.[38] From Fig. 7, it can also be concluded that the total effective rate constants for the H_2O + $^{\bullet}OH$ + CH_2X reactions (where X = S, O, NH, CH_2), are ~2–4 orders of magnitude smaller than the corresponding reactions in the absence of a water molecule. Overall, the present results indicate that the catalytic effect of a single water molecule on the $^{\bullet}OH$ + H_2CS reaction make only a negligible contribution to the gas phase removal of H_2CS from the atmosphere.

In the water assisted H_2CS + $^{\bullet}OH$ reaction, the hydrogen abstraction pathway is more dominant, which is similar to the case of the water assisted H_2CO + $^{\bullet}OH$ and CH_2NH + $^{\bullet}OH$ reactions. However, in the case of the water assisted CH_2CH_2 + $^{\bullet}OH$ reaction, the OH addition pathway is major. This situation is due to the geometries of the RCs and TSs in the water assisted H_2CS + $^{\bullet}OH$ reaction being more or less similar to those of the water assisted $^{\bullet}OH$ + CH_2O and $^{\bullet}OH$ + CH_2NH reactions, but clearly different from the $^{\bullet}OH$ + CH_2CH_2 reaction system.

The results in the present work predict that the rate of the H_2O + $^{\bullet}OH$ + H_2CS reaction is ~1–4 orders of magnitude lower than the rate of the naked reaction. However, it is interesting to see that the rate of formation of the HCS radical that occurs through the H abstraction pathway, is larger than the rate of formation of the $H_2C(OH)S$ radical that occurs from OH addition to the sp^2-carbon atom of thioformaldehyde. This is not true in the case of the bare reaction, where the rate of formation of the $H_2C(OH)S$ radical is larger compared to the rate of formation of the HCS radical. Therefore, our results reveal that while water does not catalyze the H_2CS + $^{\bullet}OH$ reaction, it still influences its chemistry by changing the branching ratios of the addition and abstraction paths. A second important element of the water assisted H_2CS + $^{\bullet}OH$ reaction in the atmosphere is that the presence of high concentrations of water results in most of the thioformaldehyde being complexed with water to form the dimer complex $H_2CS\cdots H_2O$.

We also calculated the rate constants for the H-atom abstraction channel involving the H_2CS + $^{\bullet}OH$ reaction assisted by the water dimer. The calculated bimolecular rate constants for the $^{\bullet}OH\cdots(H_2O)_2$ + H_2CS (k_7), and $H_2CS\cdots(H_2O)_2$ + $^{\bullet}OH$ (k_8) reaction paths in the temperature range between 200 and 400 K are displayed in Table S17 of the ESI.† These bimolecular rate constants were obtained by using the expressions: $k_7 = K_{eq4}k_2$ and $k_8 = K_{eq5}k_2$. Here the equilibrium constants K_{eq4} and K_{eq5} correspond to the reaction of a trimer and monomer combination to form the corresponding RC. The unimolecular rate constant is represented by k_2. The bimolecular rate constant data in Table S17 (ESI†) suggest that the rate constants for the $H_2CS\cdots(H_2O)_2$ + $^{\bullet}OH$ reaction channel are ~1 order of magnitude higher than the values for the $^{\bullet}OH\cdots(H_2O)_2$ + H_2CS reaction. For example, the rate constant for the $H_2CS\cdots(H_2O)_2$ + $^{\bullet}OH$ and $^{\bullet}OH\cdots(H_2O)_2$ + H_2CS reaction channels at 298 K were found to be 1.73×10^{-11} and 1.78×10^{-12} cm^3 $molecule^{-1}$ s^{-1}. This is mainly due to the $H_2CS\cdots(H_2O)_2$ + $^{\bullet}OH$ reaction barrier height being ~1 kcal mol^{-1} lower than the $^{\bullet}OH\cdots(H_2O)_2$ + H_2CS reaction barrier.

To assess the relative impact of the water dimer on the H-atom abstraction channel for the H_2CS + $^{\bullet}OH$ reaction in comparison with that of the same reaction in the absence and presence of a single water molecule, we also estimated the corresponding effective first order rate constants (s^{-1}) for both H_2CS + $^{\bullet}OH$ reaction assisted by the water dimer as follows: the rate for the $^{\bullet}OH\cdots(H_2O)_2$ + H_2CS and $H_2CS\cdots(H_2O)_2$ + $^{\bullet}OH$ reaction can be written as:

$$\nu_7 = k_7[^{\bullet}OH\cdots(H_2O)_2][H_2CS] \quad (26)$$

$$\nu_8 = k_8[H_2CS\cdots(H_2O)_2][^{\bullet}OH] \quad (27)$$

In eqn (26) and (27), k_7 and k_8 represent rate constants for the bimolecular $^{\bullet}OH\cdots(H_2O)_2$ + H_2CS and $H_2CS\cdots(H_2O)_2$ + $^{\bullet}OH$ reactions, respectively. The $H_2CS\cdots(H_2O)_2$, and $^{\bullet}OH\cdots(H_2O)_2$ trimer concentrations can be written in terms of the monomer and $[H_2O\cdots H_2O]$ dimer concentrations. The equilibrium for the three body formation step is given in eqn (28) and (29).

$$\nu_7 = k_7\kappa_{eq6}[H_2O\cdots H_2O][^{\bullet}OH][H_2CS] = k_7^{eff}[H_2CS] \quad (28)$$

$$\nu_8 = k_8\kappa_{eq7}[H_2O\cdots H_2O][^{\bullet}OH][H_2CS] = k_8^{eff}[H_2CS] \quad (29)$$

The $k_7^{eff} = k_7\kappa_{eq6}[H_2O\cdots H_2O][^{\bullet}OH]$ and $k_8^{eff} = k_8\kappa_{eq7}[H_2O\cdots H_2O][^{\bullet}OH]$ represent the effective first order rate constants for the $^{\bullet}OH\cdots(H_2O)_2$ + H_2CS and $H_2CS\cdots(H_2O)_2$ + $^{\bullet}OH$ reaction paths, respectively. The effective rate constant values for these two reaction pathways are given in Table S18 (ESI†). To determine these effective rate constants, we used the temperature dependent water dimer concentration (see Table S18, ESI†), the average atmospheric concentration of OH radical (10^6 molecules cm^{-3}), and the equilibrium constants (κ_{eq6}, and κ_{eq6}) for the formation of $^{\bullet}OH\cdots(H_2O)_2$ and $H_2CS\cdots(H_2O)_2$) trimer complexes from the interaction of the water dimer and a monomer reactant. The obtained effective first order rate constants (k_7^{eff} and k_8^{eff}) for both reaction pathways are given in Table S18 (ESI†). The total effective rate constants for the H_2CS + $^{\bullet}OH$ + $2H_2O$ reaction were calculated by adding the effective rate constants of the individual channels and these are also presented in Table S18 (ESI†). With the increase in altitude from 0–15 km, there is a corresponding decrease in temperature, and there is a decrease in the rate constants when the concentrations of the water dimer decrease. The concentration of the water dimer is more sensitive to the temperature, and decreases by ten orders of magnitude as the temperature drops from 400 K to 200 K (see Table S18, ESI†). The data from the table clearly suggest that the total effective rate constants for the H-abstraction channel of H_2CS + $^{\bullet}OH$ assisted by the water dimer are ~4–5 and ~5–9 orders of magnitude smaller than the H_2CS + $^{\bullet}OH$ assisted by the water, and unassisted reactions, respectively in the temperature range studied here. For example, the total effective rate constants for the H-abstraction channel of H_2CS + $^{\bullet}OH$ assisted by the water dimer, a single water molecule, and in the absence of a catalyst at 298 K were found to be 2.06×10^{-12}, 2.07×10^{-8}, and 1.50×10^{-6} s^{-1} respectively. The rate of the H-abstraction channel for the H_2CS + $^{\bullet}OH$ reaction catalyzed by the water dimer is slower, even though the barrier height of this reaction is

significantly lower (~6.7 kcal mol^{-1}) compared to the water catalyzed reaction. For this reason, we did not perform any further calculations on the addition channel of the $^{\bullet}$OH + H_2CS reaction assisted by the water dimer. The reason for the slower rate for the water dimer assisted H_2CS + $^{\bullet}$OH reaction is mainly due to the lower concentration levels of the water dimer, as its levels are smaller at lower temperatures (*i.e.* higher altitudes) in the atmosphere compared to the values for single water molecules. Therefore, we used only the single water molecule as the catalyst for the atmospheric removal of thioformaldehyde in the presence of OH radical, rather than the water dimer.

3.3. Reaction of $H_2C(OH)S^{\bullet}$ with $^3O_2$

Based on the results of the present calculations, the H_2CS + $^{\bullet}$OH addition reaction was found to be a major channel for the formation of the $H_2C(OH)S^{\bullet}$ radical product. Once formed, this radical would be anticipated to undergo further reaction with ground state oxygen ($^3O_2$) molecules which are present in large concentrations in the atmosphere.[47] We carried out detailed calculations on the $H_2C(OH)S^{\bullet}$ + $^3O_2$ reaction. The geometries of the molecules involved in this reaction were optimized at the M06-2X level in conjunction with the 6-311++G(2d,2p) basis set. The single point energy calculations were performed at the CCSD(T)/aug-cc-pVTZ//M06-2X/6-311++G(2d,2p) level of theory. The T1 diagnostic values for the reactants, intermediates, TSs, and products involved in the $H_2C(OH)S^{\bullet}$ + $^3O_2$ reaction were calculated at the CCSD(T)/aug-cc-pVTZ level and the values are displayed in Table S19 (ESI†). The data from the table suggest that the T1 diagnostic values of all the species are smaller than 0.044. This indicates that the multi-reference character in the CCSD(T) wave functions was negligible.[69] The potential energy profile involving all the stationary points for the $H_2C(OH)S^{\bullet}$ + $^3O_2$ reaction system is shown in Fig. 8. The relative energies provided in the figure were calculated at the CCSD(T)/aug-cc-pVTZ//M06-2X/6-311++G(2d,2p) level of theory with respect to the starting reactants ($(OH)CH_2S^{\bullet}$ + $^3O_2$). The optimized structures of all TSs, intermediates, and their corresponding products are shown in Fig. 9. This reaction mainly proceeds by association and direct hydrogen abstraction pathways as illustrated in Fig. 8. From the figure, it can be seen that the barrier height for abstraction of an H-atom by $^3O_2$ from the $-CH_2$ moiety of the $(OH)CH_2S^{\bullet}$ radical *via* TS9 is found to be 21.5 kcal mol^{-1} above that of the separated reactants. TS9 leads to the formation of PC8, which then proceeds to form HC(=S)OH + HO_2 as separated products. Similarly, the barrier height for the abstraction of an H-atom by an atmospheric oxygen molecule from the OH moiety of the $(OH)CH_2S^{\bullet}$ radical, followed by simultaneous formation of a single bond between the S- and O-atoms *via* TS10 (see Fig. 8) was calculated to be 54.4 kcal mol^{-1} relative to that of the starting $(OH)CH_2S^{\bullet}$ + O_2 reactants. This then proceeds to form PC9, which undergoes decomposition to yield (CH_2SO) + HO_2. Therefore, direct hydrogen abstractions through TS9 and TS10 are not feasible under atmospheric conditions, because these two channels involve high barriers that are accessible only under high temperature conditions.

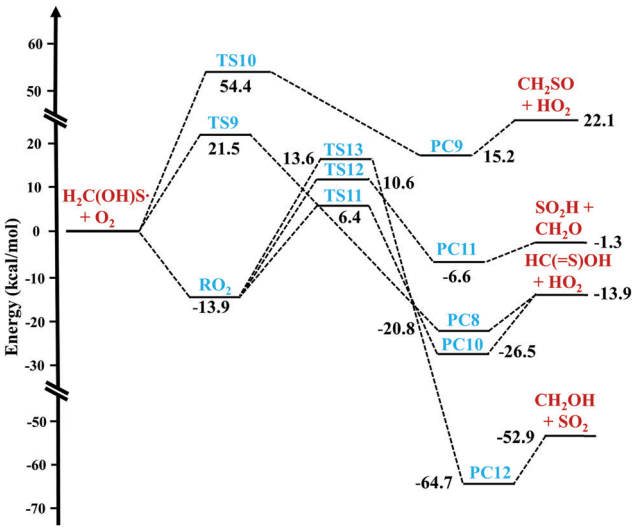

Fig. 8 Potential energy surface diagram for the $H_2C(OH)S^{\bullet}$ + $^3O_2$ reaction to form various products, obtained at CCSD(T)/aug-cc-pVTZ//M06-2X/6-311++G(2d,2p) level.

The association of $(OH)CH_2S^{\bullet}$ with $^3O_2$ is barrierless and forms a $(OH)CH_2SOO^{\bullet}$ adduct (RO2) with an energy of −13.9 kcal mol^{-1} relative to that of the starting reactants. The formed RO2 can decompose *via* three pathways: (1) elimination of HO_2 with a barrier height of 6.4 kcal mol^{-1} above that of the separated reactants through transition state (TS11). The peroxy group terminal oxygen atom in RO2 forms a bond with the H atom followed by simultaneous cleavage of the S–O single bond and formation of the C=S double bond *via* a five membered ring transition state (see Fig. 9). TS11 leads *via* PC10 to the formation of HC(=S)OH + $HO^{\bullet}{}_2$ products; (2) transfer of the H atom of the –OH group to the peroxy group O-atom, followed by C–S single bond cleavage *via* transition state (TS12), with a barrier height of 10.6 kcal mol^{-1}. The CH_2(=O) + $^{\bullet}$SOOH products are formed from the decomposition of PC11, which is formed from TS12; (3) Attack by the terminal oxygen of the peroxyl radical on the sulfur atom, forming a three membered SOO ring with simultaneous cleavage of the S–C single bond (see Fig. 8) *via* a transition state (TS13), with a barrier height of 13.6 kcal mol^{-1} above the reactants. The initial attack by the peroxyl radical leads to the formation of the more stable RSO2 (PC12) with an energy of 64.7 kcal mol^{-1} below the separated reactants ($H_2C(OH)S^{\bullet}$ + $^3O_2$). The formed PC12 undergoes unimolecular decomposition to yield $^{\bullet}CH_2OH$ + SO_2 as final products. Based on the barrier heights, unimolecular elimination of HO_2 through formation of HC(=S)OH is the major channel under atmospheric conditions. The feasibility of the other two possible channels depends on the amount of energy required to overcome the barrier heights to produce the corresponding reaction products.

The concerted elimination of HO_2 from the RO_2 radical (*i.e.* $H_2C(OH)SOO$), has a barrier of ~20.3 kcal mol^{-1} (see Fig. 8). The rate constant for the elimination was found to be 7.56×10^{-3} s^{-1} at 300 K, using the Inverse Laplace Transform (ILT) approach for handling the association reactions connected with entrance and exit channels on the PES, and RRKM

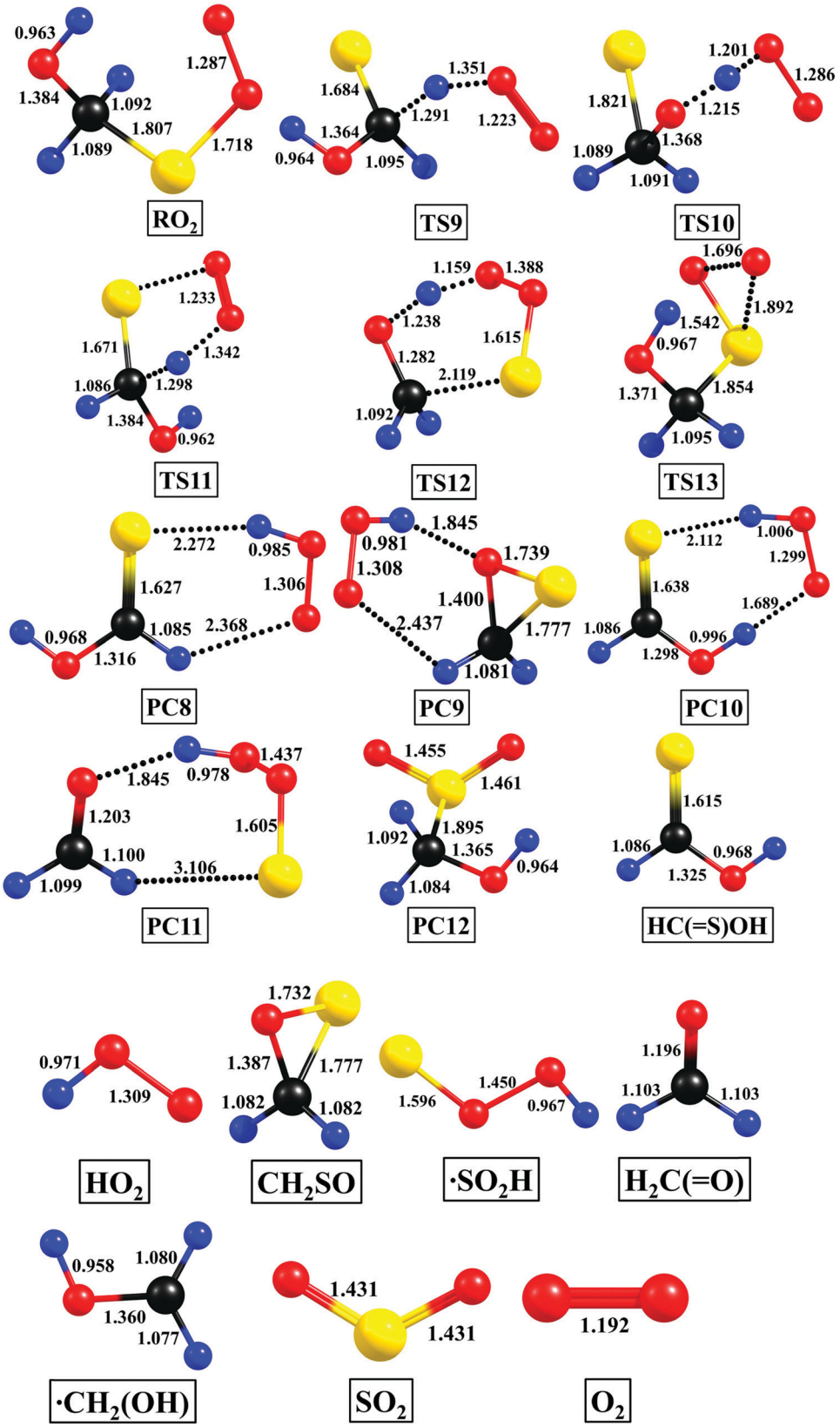

Fig. 9 Optimized geometries of the reactants, intermediates, transition states (TSs), product complexes (PCs), and products for the $H_2C(OH)S^{\bullet}$ + $^3O_2$ reaction obtained at the M06-2X/6-311++G(2d,2p) level of theory. The yellow, red, black, and blue colors denote sulfur, oxygen, carbon, and hydrogen atoms, respectively.

theory in conjunction with the Eckart tunneling method with Mesmer kinetic code.[70] These RO_2 radicals also undergo reactions with other important atmospheric trace species such as NO and HO_2 radicals, which compete with the unimolecular HO_2 elimination reaction. The bimolecular rate constants for the RO_2 + NO and RO_2 + HO_2 reactions are reported to be 8.5×10^{-12} cm^3 $molecule^{-1}$ s^{-1} and 2.0×10^{-11} cm^3 $molecule^{-1}$ s^{-1}, respectively.[71,72] Under ambient conditions, the effective rate constants for RO_2 + NO and RO_2 + HO_2 reactions were calculated to be ~ 0.7 s^{-1} and ~ 0.014 s^{-1} respectively. These values were calculated using estimates of NO and HO_2 concentrations in polluted urban areas (*i.e.* $\sim 9.0 \times 10^{10}$ molecules cm^{-3} and $\sim 7.0 \times 10^{8}$ molecules cm^{-3}, respectively).[72] Based on these values, RO_2 + NO and RO_2 + HO_2 reactions are more dominant than the HO_2 elimination reaction in polluted urban areas. The HO_2 elimination reaction is dominant only at lower concentrations of NO and HO_2 radicals in the atmosphere.

4. Conclusions

The atmospheric chemistry of the gas phase reaction of thioformaldehyde is of high importance due to its potential role as a precursor of secondary pollutants such as SO_2, thioformic acid, HO_2, and formaldehyde. We investigated the H_2CS + $^{\bullet}OH$ reaction alone and assisted by a single water molecule using CCSD(T)//M06-2X and CCSD(T)//MP2 level electronic structure calculations. Based on the reaction barrier heights, the dominant reaction pathway was found to be the addition of OH radical to the sp^2 C-atom of H_2CS in the presence and absence of a H_2O molecule (in contrast to the abstraction channel). The rate constants for water-free and water-assisted H_2CS + $^{\bullet}OH$ reactions were computed using the CVT/SCT method in the temperature range of 200 and 400 K. The rate constant data suggest that the addition reaction is $\sim$2–9 times more dominant than the abstraction path in the absence of water. Conversely, in the water assisted reaction, the abstraction channel is $\sim$3–37 times more dominant than the addition path in the studied temperature range. Nevertheless, our kinetic results indicate that a single water molecule does not exert a rate enhancement effect on the gas phase reaction of H_2CS + $^{\bullet}OH$ in the temperature range between 200–400 K. We also investigated the H-atom abstraction pathway for the H_2CS + $^{\bullet}OH$ reaction assisted by water dimer using CCSD(T)//M06-2X level. The computed barrier heights for the uncatalyzed, water-, and water dimer-assisted H-abstraction pathways for the H_2CO + OH reaction were 0.2, −5.5, and −8.2 kcal mol^{-1}, respectively. This suggests that the water dimer reduces the barrier more significantly when compared to the uncatalyzed and single water molecule catalyzed reactions. However, the kinetic results suggests that the rate of the H-atom abstraction pathway for the H_2CS + $^{\bullet}OH$ reaction assisted by the water dimer are $\sim$4–5 and $\sim$5–9 orders of magnitude smaller than the H_2CS + $^{\bullet}OH$ assisted by water, and unassisted reactions, respectively in the temperature range of 200 and 400 K. This is because the concentration of water dimer in the gas phase is negligibly under these conditions. In addition, the atmospheric oxidation of the dominant reaction product $H_2C(OH)S^{\bullet}$ with molecular oxygen ($^3O_2$) computed at the CCSD(T)/aug-cc-pVTZ//M06-2X/6-311++G(2d,2p) level was investigated. The major reaction sequence is OH radical addition to the sp^2 C-atom of H_2CS, followed by addition of $^3O_2$ to furnish the $H_2C(OH)S(OO)$ radical. Under atmospheric conditions, the important step in the unimolecular reaction of $H_2C(OH)S(OO)$ was found to be elimination of the HO_2 radical through formation of thioformic acid. Other possible reaction channels for the unimolecular isomerization of the $H_2C(OH)S(OO)$ radical yielded SO_2 and formaldehyde. The results provide further insights and improved understanding of the gas phase catalytic effect of single water molecules on important atmospheric reactions involving organosulfur compounds.

Conflicts of interest

There are no conflicts to declare.

Acknowledgements

The financial support of the National Science Foundation (grant numbers 1310350 and 1710221) to R.A.M is gratefully acknowledged. The authors thank the High-Performance Computing Center at the University at Albany-SUNY for their support.

References

1 D. R. Johnson, F. X. Powell and W. H. Kirchhoff, *J. Mol. Spectrosc.*, 1971, **39**, 136–145.
2 R. Mayer, J. Morgenstern and J. Fabian, *Angew. Chem., Int. Ed. Engl.*, 1964, **3**, 277–286.
3 D. Paquer, *Int. J. Sulfur Chem., Part B*, 1972, **7**, 269–293.
4 K. E. Krantz, A. Senning and I. Shim, *J. Mol. Struct. THEOCHEM*, 2010, **944**, 83–88.
5 E. Van Dornshuld, C. M. Holy and G. S. Tschumper, *J. Phys. Chem. A*, 2014, **118**, 3376–3385.
6 Y. C. Minh, W. M. Irvine and M. K. Brewer, *Astron. Astrophys.*, 1991, **244**, 181–189.
7 K. Willacy and T. J. Millar, *Astron. Astrophys.*, 1997, **324**, 237–248.
8 S. D. Taylor, O. Morata and D. A. Williams, *Astron. Astrophys.*, 1998, **336**, 309–314.
9 M. Agúndez, J. P. Fonfría, J. Cernicharo, J. R. Pardo and M. Guélin, *Astron. Astrophys.*, 2008, **479**, 493–501.
10 C. Comito, P. Schilke, T. G. Phillips, D. C. Lis, F. Motte and D. Mehringer, *Astrophys. J., Suppl. Ser.*, 2005, **156**, 127–167.
11 L. M. Woodney, M. F. A'Hearn, J. McMullin and N. Samarasinha, *Earth, Moon, Planets*, 1997, **78**, 69–70.
12 J. I. Moses, M. Allen and G. R. Gladstone, *Geophys. Res. Lett.*, 1995, **22**, 1597–1600.
13 R. P. Steer, *Rev. Chem. Intermed.*, 1981, **4**, 1–41.
14 D. J. Clouthier and D. A. Ramsay, *Annu. Rev. Phys. Chem.*, 1983, **34**, 31–58.

15 M. E. Jacox and D. E. Milligan, *J. Mol. Spectrosc.*, 1975, **58**, 142–157.
16 D. J. Bedwell and G. Duxbury, *J. Mol. Spectrosc.*, 1980, **84**, 531–558.
17 P. H. Turner, L. Halonen and I. M. Mills, *J. Mol. Spectrosc.*, 1981, **88**, 402–419.
18 M. Torres, I. Safarik, A. Clement and O. P. Strausz, *Can. J. Chem.*, 1982, **60**, 1187–1191.
19 D. J. Clouthier, C. M. L. Kerr and D. A. Ramsay, *Chem. Phys.*, 1981, **56**, 73–80.
20 G. Duxbury, H. Kato and M. L. Le Lerre, *Faraday Discuss. Chem. Soc.*, 1981, **71**, 97–110.
21 D. McNaughton and D. N. Bruget, *J. Mol. Spectrosc.*, 1993, **159**, 340–349.
22 E. Suzuki, M. Yamazaki and K. Shimizu, *Vib. Spectrosc.*, 2007, **43**, 269–273.
23 J. M. Flaud, W. J. Lafferty, A. Perrin, Y. S. Kim, H. Beckers and H. Willner, *J. Quant. Spectrosc. Radiat. Transfer*, 2008, **109**, 995–1003.
24 J. R. Dunlop, J. Karolczak, D. J. Clouthier and S. C. Ross, *J. Phys. Chem.*, 1991, **95**, 3045–3062.
25 D. J. Clouthier, G. Huang, A. G. Adam and A. J. Merer, *J. Chem. Phys.*, 1994, **101**, 7300–7310.
26 P. G. Burton, S. D. Peyerimhoff and R. J. Buenker, *Chem. Phys.*, 1982, **73**, 83–98.
27 J. A. Platts, S. T. Howard and B. R. F. Bracke, *J. Am. Chem. Soc.*, 1996, **118**, 2726–2733.
28 J. M. L. Martin, J. P. Francois and R. Gijbels, *J. Mol. Spectrosc.*, 1994, **168**, 363–373.
29 L. A. Curtiss, R. H. Nobes, J. A. Pople and L. Radom, *J. Chem. Phys.*, 1992, **97**, 6766–6773.
30 E. Vedejs, D. A. Perry, K. N. Houk and N. G. Rondan, *J. Am. Chem. Soc.*, 1983, **105**, 6999–7001.
31 I. Barnes, K. H. Becker and I. Patroescu, *Atmos. Environ.*, 1996, **30**, 1805–1814.
32 L. Zhu and J. W. Bozzelli, *J. Phys. Chem. A*, 2006, **110**, 6923–6937.
33 P. Arathala and R. A. Musah, *J. Phys. Chem. A*, 2019, **123**, 8448–8459.
34 M. Kumar and J. S. Francisco, *Chem. – Eur. J.*, 2017, **23**, 2522–2526.
35 M. Kumar and J. S. Francisco, *Angew. Chem., Int. Ed.*, 2016, **55**, 13432–13435.
36 A. Parandaman, C. B. Tangtartharakul, M. Kumar, J. S. Francisco and A. Sinha, *J. Phys. Chem. A*, 2017, **121**, 8465–8473.
37 R. J. Buszek, M. Torrent-Sucarrat, J. M. Anglada and J. S. Francisco, *J. Phys. Chem. A*, 2012, **116**, 5821–5829.
38 M. A. Ali, M. Balaganesh and S. Jang, *Atmos. Environ.*, 2019, **207**, 82–92.
39 C. Iuga, J. R. Alvarez-Idaboy and A. Vivier-Bunge, *J. Phys. Chem. A*, 2011, **115**, 5138–5146.
40 M. Akbar Ali, M. Balaganesh and K. C. Lin, *Phys. Chem. Chem. Phys.*, 2018, **20**, 4297–4307.
41 Y. P. Liu, G. C. Lynch, T. N. Truong, D. H. Lu, D. G. Truhlar and B. C. Garrett, *J. Am. Chem. Soc.*, 1993, **115**, 2408–2415.
42 D. G. Truhlar and B. C. Garrett, *Acc. Chem. Res.*, 1980, **13**, 440–448.
43 B. C. Garrett and D. G. Truhlar, *J. Chem. Phys.*, 1979, **70**, 1593–1598.
44 M. J. Frisch, G. W. Trucks and H. B. Schlegel, *et al.*, *Gaussian*, Gaussian Inc., Wallingford, CT, 2016.
45 M. J. Frisch, M. Head-Gordon and J. A. Pople, *Chem. Phys. Lett.*, 1990, **166**, 281–289.
46 R. Peverati and D. G. Truhlar, *Philos. Trans. R. Soc., A*, 2014, **372**, 20120476.
47 A. Parandaman, M. Kumar, J. S. Francisco and A. Sinha, *J. Phys. Chem. A*, 2018, **122**, 6266–6276.
48 A. Parandaman, J. E. Perez and A. Sinha, *J. Phys. Chem. A*, 2018, **122**, 9553–9562.
49 K. Fukui, *Acc. Chem. Res.*, 1981, **14**, 363–368.
50 H. P. Hratchian and H. B. Schlegel, in *Theory and Applications of Computational Chemistry: The First 40 Years*, ed. C. E. Dykstra, G. Frenking, K. S. Kim and G. Scuseria, Elsevier, Amsterdam, 2005.
51 J. Noga and R. J. Bartlett, *J. Chem. Phys.*, 1987, **86**, 7041–7050.
52 S. Jørgensen and H. G. Kjaergaard, *J. Phys. Chem. A*, 2010, **114**, 4857–4863.
53 N. González-García, À. González-Lafont and J. M. Lluch, *J. Phys. Chem. A*, 2006, **110**, 798–808.
54 M. Kumar and J. S. Francisco, *Proc. Natl. Acad. Sci. U. S. A.*, 2017, **114**, 864–869.
55 G. Song and J. W. Bozzelli, *J. Phys. Org. Chem.*, 2018, **31**, e3751.
56 L. Sandhiya, P. Kolandaivel and K. Senthilkumar, *Struct. Chem.*, 2012, **23**, 1475–1488.
57 B. Ruscic and J. Berkowitz, *J. Chem. Phys.*, 1993, **98**, 2568–2579.
58 B. Ruscic, *Active Thermochemical Tables (ATcT) Values Based on Ver. 1.112 of the Thermochemical Network*, Argonne National Laboratory, Argonne, IL, 2013.
59 A. S. Menon and L. Radom, *J. Phys. Chem. A*, 2008, **112**, 13225–13230.
60 M. Akbar Ali and J. R. Barker, *J. Phys. Chem. A*, 2015, **119**, 7578–7592.
61 M. E. Dunn, E. K. Pokon and G. C. Shields, *J. Am. Chem. Soc.*, 2004, **126**, 2647–2653.
62 L. Xu, N. T. Tsona, S. Tang, J. Li and L. Du, *ACS Omega*, 2019, **4**, 5805–5817.
63 T. Zhang, C. Yang, X. Feng, J. Kang, L. Song, Y. Lu, Z. Wang, Q. Xu, W. Wang and Z. Wang, *Phys. Chem. Chem. Phys.*, 2016, **18**, 17414–17427.
64 T. Zhang, X. Lan, Y. Zhang, R. Wang, Y. Zhang, Z. Qiao and N. Li, *Mol. Phys.*, 2019, **117**, 516–530.
65 D. A. McQuarrie, *Statistical Mechanics*, University Science Books, Sausalito, CA, 2000.
66 W. Zhang, B. Du and Z. Qin, *J. Phys. Chem. A*, 2014, **118**, 4797–4807.
67 C. Iuga, J. R. Alvarez-Idaboy, L. Reyes and A. Vivier-Bunge, *J. Phys. Chem. Lett.*, 2010, **1**, 3112–3115.
68 J. Zheng, S. Zhang, B. J. Lynch, J. C. Corchado, Y. Y. Chuang, P. L. Fast, W.-P. Hu, Y.-P. Liu, G. C. Lynch and K. A. Nguyen, *et al.*, *POLYRATE, version2016*, University of Minnesota, Minneapolis, MN, 2016.

69 T. J. Lee and P. R. Taylor, *Int. J. Quantum Chem., Symp.*, 1989, **36**, 199–207.
70 D. R. Glowacki, C.-H. Liang, C. Morley, M. J. Pilling and S. H. Robertson, *J. Phys. Chem. A*, 2012, **116**, 9545–9560.
71 S. M. Saunders, M. E. Jenkin, R. G. Derwent and M. J. Pilling, *Atmos. Chem. Phys.*, 2003, **3**, 161–180.
72 F. Bianchi, T. Kurtén, M. Riva, C. Mohr, M. P. Rissanen, P. Roldin, T. Berndt, J. D. Crounse, P. O. Wennberg, T. F. Mentel, J. Wildt, H. Junninen, T. Jokinen, M. Kulmala, D. R. Worsnop, J. A. Thornton, N. Donahue, H. G. Kjaergaard and M. Ehn, *Chem. Rev.*, 2019, **119**, 3472–3509.

